scientific reports

Check for updates

OPEN

Heterozygous mutation in *BRCA2* induces accelerated age-dependent decline in sperm quality with male subfertility in rats

Yashiro Motooka[1]✉, Hideaki Tanaka[1,2], Yuki Maeda[1], Misako Katabuchi[1,3], Tomoji Mashimo[4] & Shinya Toyokuni[1,5]✉

Tumor suppressor BRCA2 executes homologous recombination to repair DNA double-strand breaks in collaboration with RAD51, involving exon 11 and 27. Exon 11 constitutes a region where pathogenic variants (PVs) accumulate, and mutations in this region are known to contribute to carcinogenesis. However, the impact of the heterozygous PVs of *BRCA2* exon 11 on the life quality beyond cancer risk, including male fertility, remains unclear. Here, we established a rat model with a frameshift on the seventh BRC repeat in *Brca2* exon 11 (*Brca2*$^{+/p.T1942fs}$), which is homologous to human *BRCA2*$^{+/p.T1974fs}$, using CRISPR/Cas9 system. Our analyses revealed that the heterozygous rats with the PV in the *BRCA2* exon 11 showed increased DNA double-strand breaks and apoptosis in spermatogonia and spermatocytes, accelerated testicular germ cell loss, and deterioration in sperm quality according with aging, ultimately resulting in early male reproductive dysfunction. Of note, these alterations in testes and sperm, including DNA fragmentation in spermatozoa, were observed from completion of sexual maturation. The present findings suggest that it is crucial to consider not only cancer risk but also potential declines in reproductive capacity in men carrying *BRCA2* exon 11 PVs. Further investigation is warranted to determine whether similar traits appear in humans.

Keywords BRCA2 exon 11, Pathogenic variant, Heterozygote, Spermatogenesis, Aging, Male subfertility

Abbreviations

A	Type A spermatogonia
AO	Acridine orange
B	Type B spermatogonia
DI	Diplotene and diakinesis
BRME1	Break Repair Meiotic Recombinase Recruitment Factor 1
BSA-TBST	bovine serum albumin-Tris-buffered saline with Tween 20
DSB(s)	Double-strand break(s)
DW	Deionized water
FFPE	Formalin-fixed paraffin-embedded
GD	Gestational date
GSEA	Gene set enrichment analysis
HBOC	Hereditary breast and ovarian cancer syndrome
4-HNE	4-hydroxy-2-nonenal
HR	Homologous recombination
HRP	Horseradish peroxidase
HSF2BP	Heat Shock Transcription Factor 2 Binding Protein
IHC	Immunohistochemistry (-chemical)

[1]Department of Pathology and Biological Responses, Nagoya University Graduate School of Medicine, 65 Tsurumai-cho, Showa-ku, Nagoya 466-8550, Japan. [2]Department of Obstetrics and Gynecology, Nagoya University Graduate School of Medicine, 65 Tsurumai-cho, Showa-ku, Nagoya 466-8550, Japan. [3]Department of Obstetrics and Gynecology, Faculty of Life Sciences, Kumamoto University, 1-1-1, Honjo, Chuo-ku, Kumamoto City, Kumamoto 860-8556, Japan. [4]Laboratory Animal Research Center, Institute of Medical Science, The University of Tokyo, Tokyo, Japan. [5]Center for Low-temperature Plasma Sciences, Nagoya University, Furo-cho, Chikusa-ku, Nagoya 464-8603, Japan. ✉email: motooka@med.nagoya-u.ac.jp; toyokuni@med.nagoya-u.ac.jp

JS	Johnsen's score
L	Leptotene
M	Metaphase
MEILB2	Meiotic localizer of BRCA2
mut	*Brca2*$^{p.T1942fs}$ mutant
8-OHdG	8-hydroxy-2'-deoxyguanosine
P	Pachytene
PARP	Poly (ADP-ribose) polymerase
PCR	Polymerase chain reaction
PV(s)	Pathogenic variant(s)
PVDF	Polyvinylidene fluoride
R	Resting spermatocyte(s)
RIPA	Radioimmunoprecipitation assay
ROI	Region of interest
SCSA	Sperm chromatin structure assay
SD rat	Sprague-Dawley rat
SDS-PAGE	Sodium dodecyl sulfate-polyacrylamide gel electrophoresis
T	Transition form
wt	Wild-type

BRCA2 DNA repair associated (BRCA2) is a tumor suppressor gene, encompassing 85,183 base pairs with 27 exons and translating into a protein of 3,418 amino acids in humans. This gene contains the specific regions highly conserved between humans and rodents, including BRC repeats, DNA-binding region and C-terminal region, which are believed to harbor important functions[1]. Indeed, BRCA2 forms a complex with RAD51, using BRC-repeats domains and C-terminal RAD51-binding domain encoded by exon 11 and 27, respectively, to facilitate homologous recombination (HR) repair of DNA double-strand breaks (DSBs)[2–4]. Germline pathogenic variants (PVs) in *BRCA2* are associated with an increased risk of various cancers. The germline PVs in *BRCA2* are found in 0.17–1.31% of the population[5,6], frequently found in exon 11, especially the latter half of the region[7,8]. *BRCA2* PVs in the homozygous state are responsible for Fanconi anemia, complementation group D1, which carries a 97% probability of causing a malignancy, including acute myeloid leukemia, medulloblastoma, and Wilms tumor, by the age of 5.2 years[9,10]. Heterozygous *BRCA2* PVs are also associated with an elevated risk of cancers in the breasts, ovaries, prostate, and pancreas, constituting a major portion of Hereditary Breast and Ovarian Cancer Syndrome (HBOC)[5,11]. Of note, the cancer risk in male *BRCA2* PV carriers increases after the age of 45 years, when many men have finished their reproduction[11,12]. Clinically, male *BRCA2* PV carriers are identified by genetic tests upon diagnosis of male breast cancer, or when poly (ADP-ribose) polymerase (PARP) inhibitor treatment is considered for prostate or pancreatic cancer. More commonly, these diagnoses are made, following the identification of a *BRCA2* PV within a family[13].

In addition to cancer risk, *BRCA2* has been reported to influence male reproductive function in situations where there is no or scarce expression of normal BRCA2 protein in the testis. Aspermatogenesis was observed in the rats homozygous for the allele representing truncated BRCA2 protein[14]. Additionally, meiotic impairment and germ cell degeneration were observed in the mice with deficient murine *Brca2* but supplemented with human *BRCA2*, which exhibited undetectable expression of BRCA2 protein in the gonads[15,16]. Furthermore, recent studies have revealed that the domain encoded by *BRCA2* exon 12–13 plays a critical role in meiosis by forming a complex with Heat Shock Transcription Factor 2 Binding Protein (HSF2BP)/Meiotic localizer of BRCA2 (MEILB2) and Break Repair Meiotic Recombinase Recruitment Factor 1 (BRME1)[17–20]. However, the influence of heterozygous PVs in *BRCA2* on male reproductive function, including sperm quality, has not been fully elucidated yet.

Here, we engineered a Jcl: SD (Sprague-Dawley) rat model with a *Brca2* mutation using CRISPR/Cas9 genome editing to study the male fertility and demonstrated that a frameshift mutation in the 7th BRC repeat of *Brca2* exon 11 leads to a decline in germ cell numbers and disorders during spermatogenesis, resulting in male subfertility. The homozygous mutants were embryonic lethal by gestational date (GD) 8.5. The heterozygous mutants developed normally but exhibited increased DNA DSBs and apoptosis in testicular germ cells, along with deteriorating sperm quality as they aged, eventually leading to early reproductive dysfunction. These findings suggest that the male carriers of *BRCA2* exon 11 PVs are at risk for infertility. It is urgently needed to evaluate whether a similar decline in male reproductive potential occur in humans.

Results

Allele with a frameshift in *Brca2* Exon 11 exhibits poor transmission to the F1 generation in rats

We generated *Brca2* mutant Jcl: SD rats harboring a stop codon in exon 11, using genome editing by CRISPR/Cas9 system. Considering that germline PVs in *BRCA2* are predominantly found in the latter half of exon 11[7,8] and that 7th BRC repeat encoded by exon 11 is conserved between humans and rats, we designed the guide RNA targeting the 7th BRC repeat (Fig. 1a). Guide RNA and Cas9 mRNA were injected into Jcl: SD rat zygotes, which were then transplanted to a pseudo-pregnant female (Fig. 1b). We obtained 4 male and 6 female founder mutant rats with a frameshift mutation causing a premature stop codon. However, most of these mutant alleles were not successfully passed on to the F1 generation through breeding with wild-type Jcl: SD rats, resulting in natural selection of a single mutant type, *Brca2*$^{+/p.T1942fs}$ (ENSRNOT00000001475.8: c.5825_5847del, p.T1942Kfs*8; *Brca2*$^{wt/mut}$), which is homologous to human *BRCA2*$^{+/p.T1974fs}$ (Fig. 1c, d, e, f, g). After confirming the absence

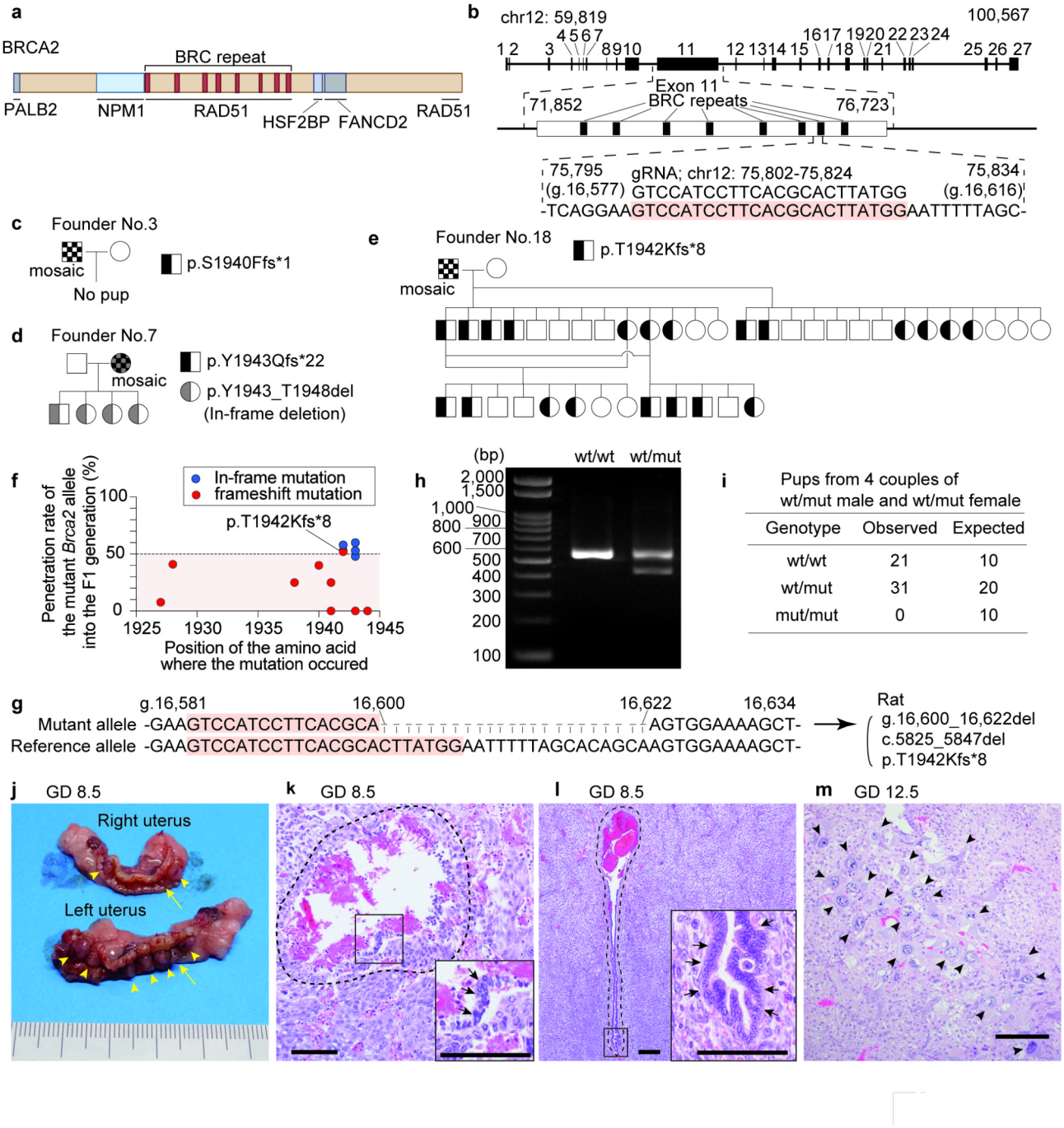

Fig. 1. Design and the founders of Jcl: SD Brca2 (Here only Brca2 to be italic, please) mutant rats harboring a frameshift on exon 11 with embryonic lethality in the homozygotes. (**a**) Structure of rat BRCA2 protein. (**b**) Structure of rat *Brca2* and guide RNA used for genome editing. (**c**-**e**) The pedigree of founder rats. (**f**) A graphical summary of the inheritance rate of the mutant *Brca2* allele in the F1 generation, categorized by the site of the mutated amino acid. Founder rats that produced no pups are also plotted as 0%. This figure indicates that the frameshift mutation in *Brca2* is less likely to be inherited to the subsequent generation. (**g**) The nucleotide sequence of the modified region within the *Brca2* gene and their notation. (**h**) Representative result of genotyping PCR of the $Brca2^{wt/wt}$ and $Brca2^{wt/mut}$. (**i**) Contingency table showing observed and expected counts of offspring with each genotype from 4 pairs of $Brca2^{wt/mut}$ male rats and $Brca2^{wt/mut}$ female rats. (**j**) Macroscopic image of uteri from a pregnant female taken at GD 8.5. Arrow heads, conceptuses; arrows, malformed conceptuses. (**k, l**) Representative histology of dying conceptuses (**k**) and live conceptuses (**l**) at GD 8.5 (arrows, embryonic components; bar = 200 μm). In the dying conceptus, cell detachment, loss of tissue continuity and hemorrhage are observed. (m) Microscopic image showing remnant of pregnancy observed at GD 12.5 (arrow heads, trophoblastic cells; bar = 200 μm). Fetal components are absent, and cluster of trophoblastic cells with large nuclei, some of which are syncytialized, are observed.

of mutations in the off-target areas (Figure S1), this specific strain was maintained as male heterozygotes by breeding with wild-type Jcl: SD female rats (CLEA Japan, Inc., Tokyo, Japan).

Brca2$^{mut/mut}$ rats are embryonic lethal

To investigate the heritability of the *Brca2*^{mut} allele, we analyzed the genotypes of offspring from 4 pairs of *Brca2*$^{wt/mut}$ male and female rats. Genotyping using PCR analysis revealed a complete absence of *Brca2*$^{mut/mut}$ pups, with a ratio of wild-type to heterozygotes being 21: 31 (Fig. 1h, i), suggesting that the homozygotes are embryonic lethal. Furthermore, to determine at which stage of development embryonic lethality occurs, we evaluated the uteri of pregnant *Brca2*$^{wt/mut}$ female rats mated with *Brca2*$^{wt/mut}$ males at GD 7.5, 8.5, 9.5, and 12.5 ($n=1$ for each stage), defining the post-coital morning as day 0. Here, we sectioned the tissue at four micrometers intervals and examined all tissue sections. At GD7.5, no implanted embryos were observed. At GD 8.5, we observed five perishing conceptuses exhibiting sings of tissue degeneration, including discontinuity in the epithelium-like cells, loss of structural cohesion, and hemorrhage. At GD 9.5 four perishing conceptuses with similar morphological findings were noted (Fig. 1j, k, l)[21,22]. At GD 12.5, two clusters of trophoblast cells without fetal components were observed and considered to be remnants of pregnancies that had resulted in lethality (Fig. 1m).

Testicular BRCA2 expression is decreased in *Brca2*$^{wt/mut}$ rats

To evaluate the differences in BRCA2 protein expression, we conducted immunohistochemical (IHC) analysis on formalin-fixed paraffin-embedded (FFPE) testicular specimens of *Brca2*$^{wt/wt}$ and *Brca2*$^{wt/mut}$ rats. Seminiferous epithelial cells were morphologically classified into fourteen stages for evaluation, based on the cycle of the seminiferous epithelium[23] (Fig. 2a, b). With this evaluation, it was difficult to clearly differentiate resting spermatocyte from type-A spermatogonia in stage VIII tubules, suggesting that some type-A spermatogonia may be included when evaluating resting spermatocytes. Despite this limitation, our observations revealed strong positive expression of BRCA2 and phosphorylated BRCA2 in spermatocytes in wild-type stage V to XIV (Fig. 2c, e). In contrast, in *Brca2*$^{wt/mut}$ rats, the expression of BRCA2 was lower in most stages from spermatogonia to spermatocytes in comparison to *Brca2*$^{wt/wt}$ (Fig. 2d, Figure S2a). The expression of phosphorylated BRCA2 was also significantly lower or showed a tendency to be lower across many stages, from spermatogonia to spermatocytes (Fig. 2f, Figure S2b).

Brca2 mutant allele induces alteration neither in splicing variants nor production of truncated BRCA2 protein

To evaluate the alteration in *Brca2* splicing variants, JunctionSeq analysis was performed, based on RNA-seq from the testes of 10-week-old rats (*Brca2*$^{wt/wt}$, $n=3$; *Brca2*$^{wt/mut}$, $n=3$). This analysis revealed no significant changes in the splicing variants (Fig. 3a, b). Furthermore, immunoblots of testicular lysates from 11-week-old rats using three different anti-BRCA2 antibodies, each of which recognizes regions upstream of mutation point, downstream of mutation point and phosphorylated BRCA2, respectively, showed a trend of decreased expression of BRCA2 in *Brca2*$^{wt/mut}$. However, no new bands indicative of changes in splicing or the formation of truncated BRCA2 proteins were observed (Fig. 3c, d, e, f, g, h, i and Figure S3).

Young adult *Brca2*$^{wt/mut}$ male rats present a decrease in testicular germ cells and secondary male subfertility

As an additional analysis on the splicing variants by RNA-seq of the testes from 10-week-old rats (*Brca2*$^{wt/wt}$, $n=3$; *Brca2*$^{wt/mut}$, $n=3$), a pathway analysis using Gene Set Enrichment Analysis (GSEA) was performed. The results revealed that many gene sets related to male infertility were enriched even in a heterozygous deficient state of *Brca2* (Fig. 4a, b). Consequently, we evaluated male reproductive capacity between 6 and 8 months of age and assessed pathological changes in the testes and spermatozoa at both 11-week-old and 8-month-old. It is established that all male rats at 11-weeks old (adolescent age) have just completed sexual maturation whereas male rats at 8-month- old (young adult age) are equivalent to a human age of 20–23 years[24,25] (Figs. 4c and 5a).

In the evaluation of reproductive efficiency, *Brca2*$^{wt/wt}$ males showed no significant decline in reproductive performance between 6 months of age and 7 months of age whereas *Brca2*$^{wt/mut}$ males exhibited a decline in reproductive ability at 7 months of age compared to that at 6 months of age (paired *t*-test: *Brca2*$^{wt/wt}$, $P=0.445$; *Brca2*$^{wt/mut}$, $P=0.022$) (Fig. 4c, d).

Although no differences in body weight or total testicular weight were observed between *Brca2*$^{wt/wt}$ and *Brca2*$^{wt/mut}$ males (Fig. 5b, c), several pathological findings were observed in the testes from *Brca2*$^{wt/mut}$ group. In the evaluation of a germ cell marker, DEAD-Box Helicase 4 (DDX4) was positively stained in spermatocytes and spermatids in stage 1–3, Golgi phase; stage 4–7, cap phase and stage 8, beginning of acrosome phases (Fig. 5d). *Brca2*$^{wt/wt}$ seminiferous tubules exhibited uniform staining pattern of DDX4 whereas *Brca2*$^{wt/mut}$ showed patchy pattern, suggesting the presence of shedding germ cells. Furthermore, a greater decrease in DDX4-positive germ cells was observed in *Brca2*$^{wt/mut}$ at 8-month-old in comparison to *Brca2*$^{wt/wt}$ (Fig. 5d, e, f). Furthermore, morphological evaluation of spermatogenic function with Johnsen's score (JS) revealed that the JS of *Brca2*$^{wt/mut}$ males tended to be lower than *Brca2*$^{wt/wt}$ at 11-week-old and that *Brca2*$^{wt/mut}$ males showed a drastic decline in JS by 8-month-old whereas *Brca2*$^{wt/wt}$ males maintained high scores throughout the period. Detailed analysis showed that even at a younger age, *Brca2*$^{wt/mut}$ exhibited a higher fraction of JS-7 seminiferous tubules, tubules with no spermatozoa but many spermatids present. According with aging, a greater proportion of tubules exhibited poorer spermatogenic quality, including JS-1, -2 and −3, which have no cells, only Sertoli cells or spermatogonia as the only germ cell, respectively, in *Brca2*$^{wt/mut}$ rats (Fig. 5g, h, i, j).

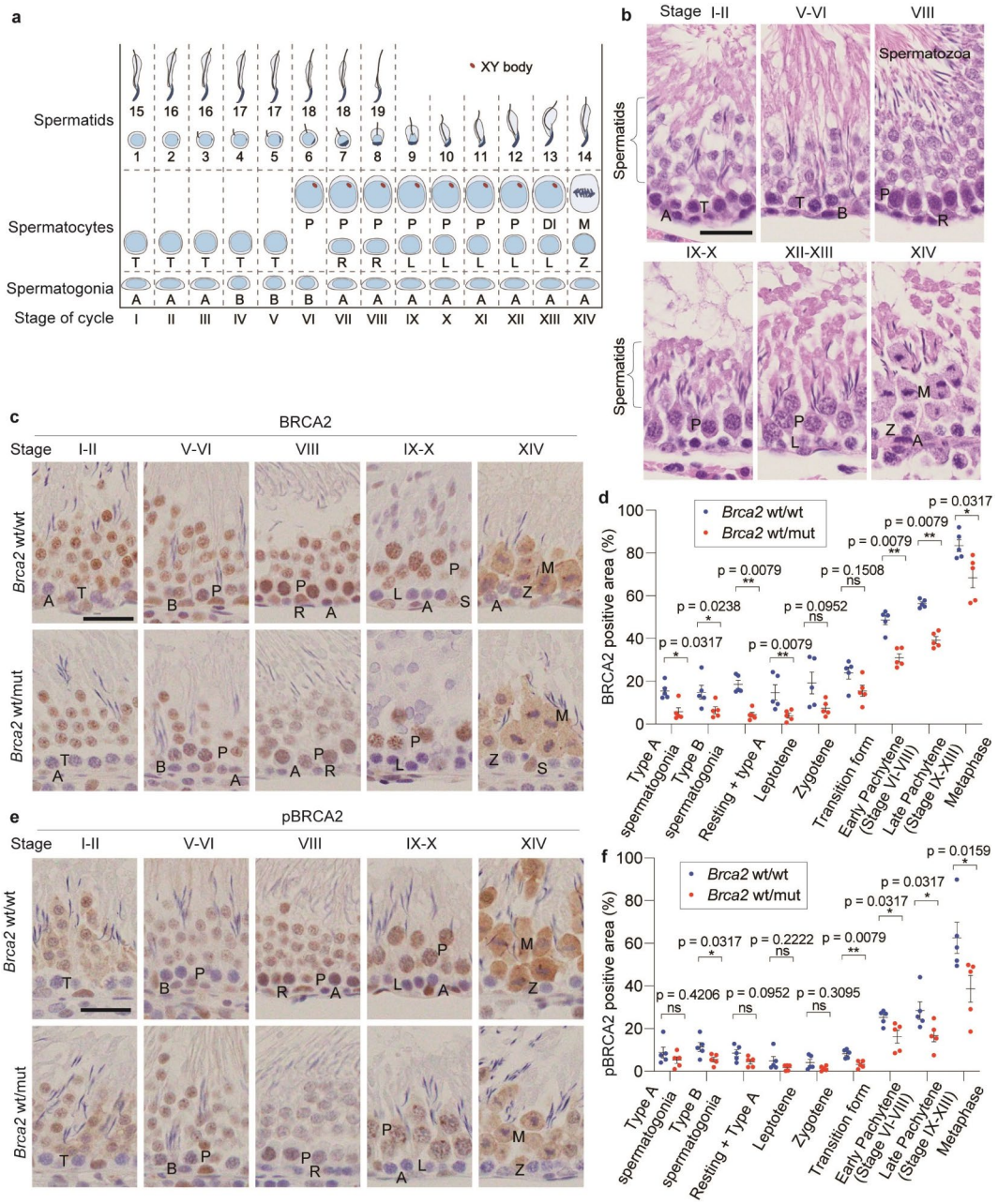

Fig. 2. BRCA2 expression is decreased in *Brca2*$^{wt/mut}$ spermatocytes. (**a**) The schematic of the stages of the seminiferous epithelium and XY body formation in rats. A, type A spermatogonia; B, type B spermatogonia; R, resting spermatocytes; L, leptotene; T, transition form; P, pachytene; DI, diplotene and diakinesis; M, metaphase. (**b**) Typical histological images of each stage of seminiferous epithelium in rats (bar = 30 μm). (**c**, **d**, **e**, **f**) Typical immunohistochemistry images of BRCA2 (E2082-L2106) and phosphorylated BRCA2 (Ser2095) (bar = 30 μm), along with quantitative analysis ($n = 5$; with at least 10 fields taken randomly with x20 magnification were analyzed per individual), indicate that BRCA2 and phosphorylated BRCA2 were primarily expressed in spermatocytes from stages VI to XIV, labeled as early Pachytene (stage VI-VIII), late Pachytene (stage IX-XIII), and Metaphase (stage XIV). The expression of BRCA2 and phosphorylated BRCA2 tended to be weaker in *Brca2*$^{wt/mut}$ spermatogonia and spermatocytes compared to *Brca2*$^{wt/wt}$ across multiple stages.

Brca2$^{wt/mut}$ testicular germ cells exhibit accumulation of DNA DSBs and increase in apoptosis

To assess the etiology of decreased germ cells, we evaluated DNA DSBs and apoptosis in testicular germ cells. IHC analysis of γH2AX revealed significant accumulation of DNA DSBs in the spermatogonia and spermatocytes of *Brca2*$^{wt/mut}$ rats during type A spermatogonia (stage IX-XIV), type B spermatogonia (stage IV-VI), resting spermatocytes period (stage VIII), leptotene phase (stage IX-XIII), zygotene phase (stage XIV) and early pachytene phase (stage VI-VIII). Furthermore, a tendency of increase in γH2AX was found during transition phase (stage I-V) and late pachytene phase (stage IX-XIII)[23] both at 11 weeks and 8 months of age

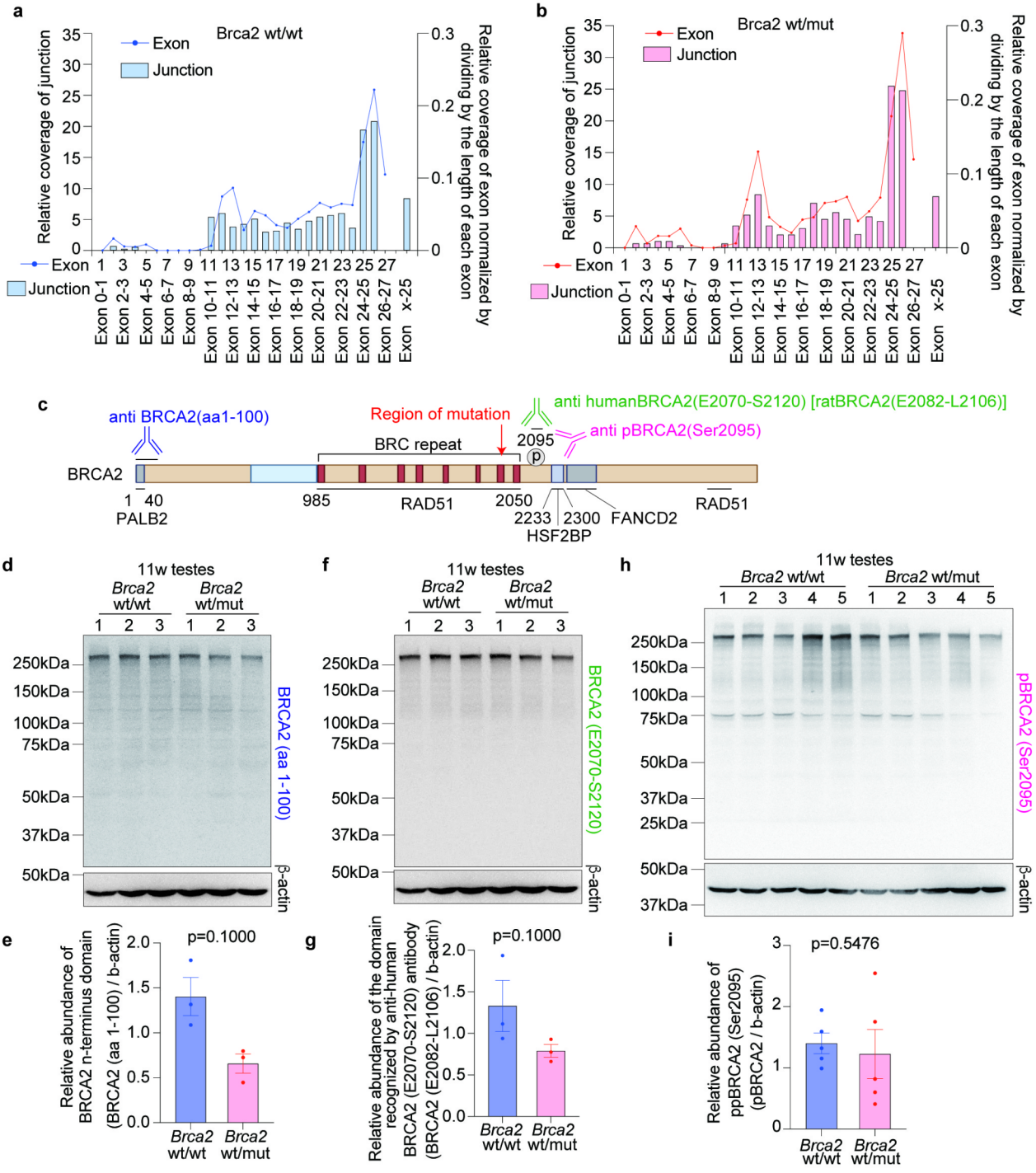

(Fig. 6a, b, c, d). On the other hand, oxidative stress markers, including 8-hydroxy-2'-deoxyguanosine (8-OHdG) and 4-hydroxy-2-nonenal (4-HNE)[26,27], exhibited no significant differences between *Brca2*$^{wt/wt}$ and *Brca2*$^{wt/mut}$ (Figure S4). Therefore, the increase in γH2AX could be the result of the accumulation of unrepaired DNA DSBs induced by the physiological level of reactive oxygen species[28].

TUNEL assay at 11 weeks of age revealed almost no positive cells in the seminiferous tubules of *Brca2*$^{wt/wt}$ rats whereas TUNEL-positive cells were frequently observed in the seminiferous tubules of the *Brca2*$^{wt/mut}$ rats, especially in the tubules classified as JS-7 or lower (Fig. 6e). To enhance accuracy of the evaluation, seminiferous tubules classified as JS-7 or lower, which are difficult to be categorized in term of the stage of seminiferous cycle, were excluded from the quantificational analysis. Subsequent stage-specific analysis demonstrated that the proportion of TUNEL-positive cells was higher in *Brca2*$^{wt/mut}$ than in *Brca2*$^{wt/wt}$ in stages I-VII, VIII and IX-XIII across spermatogonia, spermatocytes and spermatids (Fig. 6f, g, h, Figure S5).

◀**Fig. 3**. *Brca2*$^{wt/mut}$ induces neither alterative splicing variant nor different-sized BRCA2 protein in testis. (**a, b**) Analysis of splicing variant based on RNA-seq with JunctionSeq analysis (*Brca2*$^{wt/wt}$ testes, $n=3$; *Brca2*$^{wt/mut}$ testes, $n=3$). The line graph describes the relative coverage of exons normalized by dividing by the length of each exon whereas the bar graph represents the relative coverage of junction of exons. This analysis revealed no statically significant changes in the splicing variants between *Brca2*$^{wt/wt}$ and *Brca2*$^{wt/mut}$. (**c**) Diagram of the regions recognized by the anti-BRCA2 antibodies used in the immunoblot. We used an antibody against the first 100 amino acids of BRCA2; BRCA2(aa1-100), an antibody against the region from Glutamic acid at position 2070 to Serine at position 2120 on human BRCA2 (corresponding to positions 2082 to 2106 in rat BRCA2); BRCA2(E2070-2120), and an antibody against BRCA2 phosphorylated at Serine 2095; pBRCA2(Ser2095). In other words, one antibody recognizes the N-terminal side of the mutant point, while the other two recognize the C-terminal side. (**d, e, f, g, h, i**) Images of the immunoblot bands of testes lysates and their quantification results. The evaluation of BRCA2 (E2082-L2106) was conducted by reprobing the membrane used for the assessing of N-terminal domain of BRCA2 after stripping the antibody with an acidic pH protocol and confirming the removal of the antibody using Chemi-Lumi One Ultra. The predicted band size for BRCA2 (aa1-100) is 384 kDa. Uncropped images are available in Figure S2.

Brca2$^{wt/mut}$ rats exhibit decreased sperm quality in the adolescent period with age-dependent exacerbation

Considering the observed decline in the reproductive capacity and the pathological findings in *Brca2*$^{wt/mut}$ testes, we finally evaluated the spermatozoa. The count and vitality of spermatozoa in *Brca2*$^{wt/mut}$ were lower than in *Brca2*$^{wt/wt}$ both at 11-week-old and 8-month-old (Fig. 7a-d). Regarding sperm motility, the fractions of progressive and non-progressive spermatozoa were decreased with an increase in arrest spermatozoa in *Brca2*$^{wt/mut}$ by 8 months (Fig. 7e). Furthermore, a higher proportion of spermatozoa with abnormal head was observed in 11-week-old *Brca2*$^{wt/mut}$ males whereas abnormalities in the tail of spermatozoa were noted at 8-month-old (Fig. 7f, g). To assess DNA fragmentation, we employed the Sperm Chromatin Structure Assay (SCSA) due to its superior sensitivity and specificity as a tool for identifying male infertility[29]. The SCSA results indicated that spermatozoa from *Brca2*$^{wt/mut}$ males exhibited a higher ratio of DNA fragmentation than those from *Brca2*$^{wt/wt}$ even at 11 weeks (Fig. 7h, i, Figure S6).

Discussion

The present study reports the phenotype of a rat model harboring the *Brca2* exon 11 mutation, generated by CRISPPR/Cas9 genome editing in Jcl: SD rats. The engineered mutant allele results in a p.T1942fs mutation in the region of 7th BRC repeats, which is homologous to the p.T1974fs mutation in human *BRCA2*. The homozygotes were embryonic lethal by GD8.5. In contrast, the heterozygotes revealed normal development. However, these heterozygotes exhibited a decline in sperm quality as early as adolescent age (11 weeks), with further deterioration and a decrease in reproductive efficacy observed by young adult age (8 months).

Thus far, many mouse models with *Brca2* mutation have been generated, including 51 mutation alleles and 92 mouse strains or lines[30]. However, despite the Organization for Economic Cooperation and Development (OECD) recommending rats over mice for carcinogenesis experiments of chemicals[31], there have been only one *Brca2* mutant rat model available. This existing rat model, generated through random mutation approach by *N*-ethyl-*N*-nitrosourea, carries a mutation between the 2nd and 3rd BRC repeat in exon 11 [14,32]. In contrast, the current rat model harbors a mutation in the 7th BRC repeat, located at the latter half of *Brca2* exon 11, a region where germline PVs are frequently observed in humans[7,8]. Consequently, we propose that our model offers a more effective experimental platform, not only for elucidating the molecular biological functions of BRCA2 but also for demonstrating the molecular mechanisms of carcinogenesis in clinical *BRCA2* PVs carriers.

Reportedly, certain *BRCA2* PVs can lead to the production of splicing variants or truncated proteins. The former could attenuate the impacts of PVs whereas the latter may exert dominant negative effects[33–36]. However, in our rat testes, we observed no apparent alterations in the formation of either splicing variants or truncated proteins. Considering this observation alongside the reduction in both BRCA2 and phosphorylated BRCA2 in seminiferous tubules with immunostaining, the phenotypic manifestations observed in this rat model are likely due to a decrease in the expression of full-length BRCA2.

In the homozygotes, we observed embryonic lethality by GD 8.5 in this rat model. Similar findings were reported in the studies on *Brca2* exon 11 mutant mouse models, where 80–100% of homozygotes were found to be embryonic lethal between GD 8.5–9.5 [37]. Reportedly, developmental dates vary between rats and mice, with rat embryos at GD 8.5 considered equivalent to mouse embryos at GD 7-8.5 [21]. Consequently, we believe that the embryonic lethality observed in our rat model is either equivalent to, or occur at an earlier stage than, that reported in mice.

In the heterozygotes, normal development was observed. However, age-accelerated deteriorating sperm quality, testicular germ cell degeneration and a decrease in male reproductive efficacy were noted in this rat model. Concerning the relationship between *Brca2* and male infertility, previous studies on genetically engineered models in rats and mice primarily focused on the effects of no or poor expression of normal BRCA2 protein in the testes, leading to testicular germ cell degeneration, aspermatogenesis or meiotic defects[14–16]. Of note, our study extended these observations by evaluating sperm quality parameters and tracking trends in actual litter sizes, thereby the first report to demonstrate that even heterozygous mutations in *Brca2* contribute to male infertility.

Since DNA fragmentation in spermatozoa is inversely associated with sperm count and vitality, and is positively associated with the fraction of abnormal sperm[38–41], we propose that DNA fragmentation in spermatozoa is a

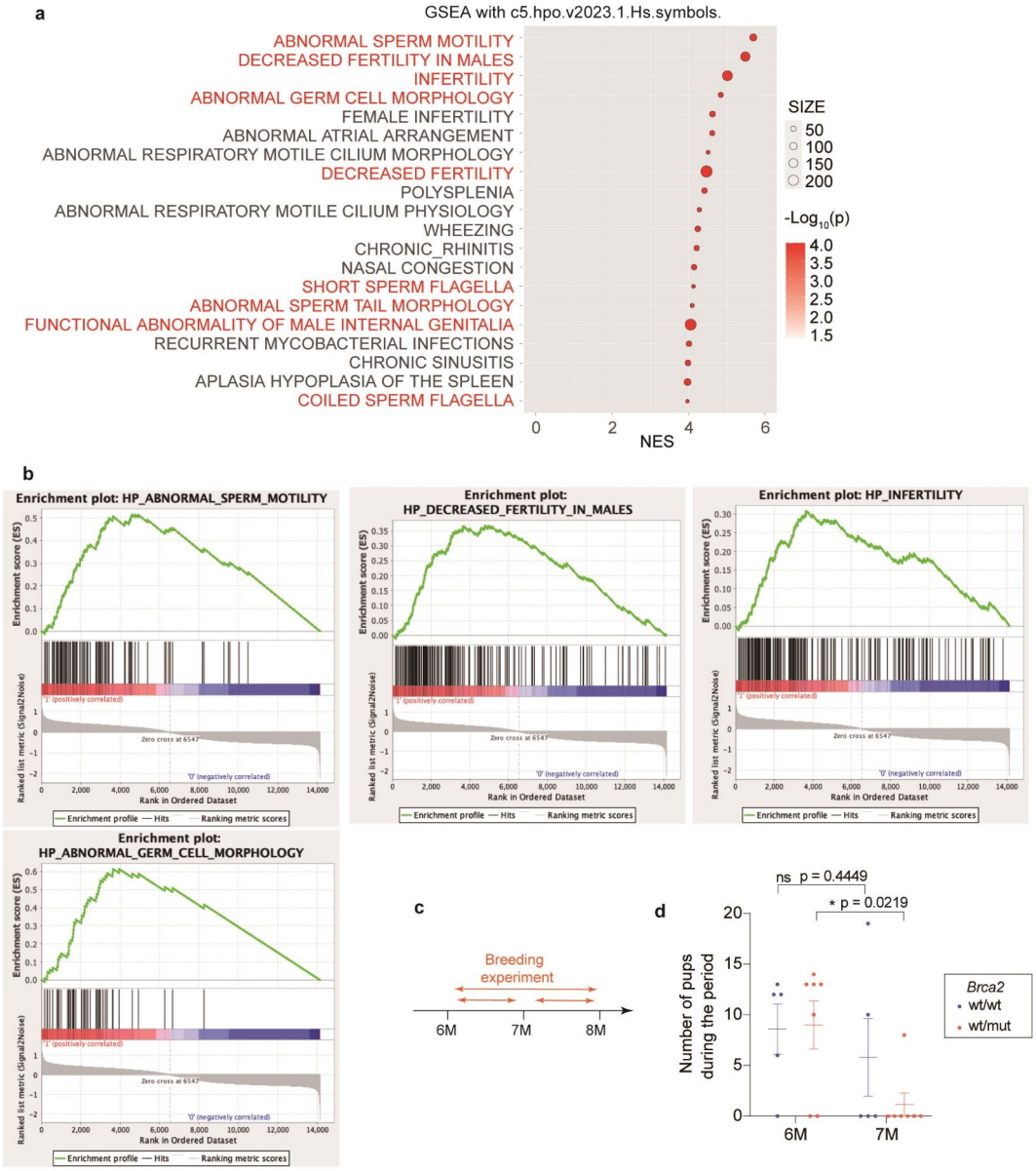

Fig. 4. *Brca2*$^{wt/mut}$ male rats contribute to rapid decline of litter size according with aging after mating with a ***Brca2***$^{wt/wt}$ female. (**a**) Top enriched gene sets in *Brca2*$^{wt/mut}$ testes compared to *Brca2*$^{wt/wt}$ by GSEA on testes from 10-week-old rats using gene set of "Human Phenotype Ontology" ($n=3$). (**b**) Enrichment plots of the gene sets associated with male infertility. (**c**) Design of experiments evaluating the reproductive efficiency. (**d**) Trends of reproductive efficiency. *Brca2*$^{wt/mut}$ male rats exhibited significant decrease in reproductive efficiency at 7 months of age in comparison to those of 6 months old whereas *Brca2*$^{wt/wt}$ males did not show a significant decrease (*Brca2*$^{wt/wt}$, $n=5$; *Brca2*$^{wt/mut}$, $n=7$).

pivotal event in the observed deterioration of spermatozoa in *Brca2*$^{wt/mut}$ rats. Considering the absence of an increase in oxidative stress, we believe that the core of the pathologic processes for this DNA fragmentation of spermatozoa is the accumulation of DNA DSBs that occur physiologically but remain unrepaired in the germ cells of the testes due to diminished BRCA2 expression. Furthermore, we understand that this accumulation of DNA DSBs in germ cells lead to an increase in the loss of testicular germ cells due to apoptosis. We conclude that these changes, compounded by increased DNA fragmentation in sperm associated with aging[42], eventually lead to a decrease in reproductive efficiency in young adults.

Among our present findings, the observation that DNA fragmentation of spermatozoa begins at an adolescent age in heterozygous *Brca2*$^{wt/mut}$ rats has important implications for clinical application, although verification in humans is necessary. Given that DNA fragmentation in human spermatozoa is associated with an fall in implantation rate[43] and an increase in early abortion rate[40], strategic cryopreservation of sperm at a young age would emerge as a logical option for male carriers of *BRCA2* exon 11 PVs to circumvent the age-related decline in the sperm quality observed in our rat model.

This study has limitations regarding the information on the natural course of this genetically engineered rat model, such as lifetime, cancer probability, lifetime trends of body weight, pathological states other than infertility at present. The evaluation of the natural course and cancer susceptibility is currently in progress with or without carcinogen(s) in our rat *Brca2*$^{wt/mut}$ model.

In conclusion, we engineered a novel *Brca2* mutant Jcl: SD rat model using a CRISPR/Cas9-induced frameshift in the 7th BRC repeat of exon 11, where human *BRCA2* PVs are frequently observed. The homozygotes were embryonic lethal. The heterozygotes exhibited normal development. However, male heterozygotes demonstrated increased DNA DSBs in spermatocytes, a higher population of apoptotic germ cells, a greater fraction of spermatozoa with DNA fragmentation, and decreased sperm count and vitality even at the adolescent age. Furthermore, they displayed reduced testicular germ cells at the young adult age, leading to male subfertility. These findings underscore the importance of investigating human male infertility from the viewpoint of *BRCA2* PVs.

Methods

Animal experiments

All procedures were approved by the Institutional Animal Care and Use Committee of University of Tokyo (PA19-89) and Nagoya University Graduate School of Medicine (M220305-002, M230297-002). This study was conducted in accordance with ARRIVE guidelines, from experimental planning, sample size determination, and random group allocation to the reporting of results and discussion, in order to enhance the transparency and reproducibility of the animal experiments. We confirm that all methods were performed in accordance with the relevant guidelines and regulations and that this study does not include research involving human participants. We engineered *Brca2* mutant *Jcl: SD* rats with a frameshift mutation in exon 11 through CRISPR/Cas9 genome editing. In brief, *Jcl: SD* rat fertilized eggs (CLEA Japan, Inc.) were injected with guide RNA and Cas9 mRNA, then implanted into pseudo-pregnant females, which produced 4 male and 6 female founder mutant rats (Table 1). These rats were mated with wild-type *Jcl: SD* rats. However, most of the mutant alleles were not inherited to the F1 generation, leading to natural selection of a single mutant type, *Brca2*$^{+/p.T1942fs}$ (*Brca2*$^{wt/mut}$). Following confirmation of no off-target mutations as described below, males of the selected strain were maintained by breeding with wild-type *Jcl: SD* female rats. To assess the male reproductive capacity, 6-month-old males were mated with 10-week-old females in a pair for 2 months, and the litter size was monitored. For the evaluation of testes and sperm, 11-week-old unmated rats and 8-month-old rats, which were used for the analysis of litter size and separated from the female for 7 days, were used. Testes and cauda epididymis were excised immediately after euthanasia with isoflurane, weighed and used for further analysis as described below.

Genotyping with PCR and Sanger sequencing for genetic mutation analysis

Primers used in this study are summarized in Table S1. DNA was extracted from the excised tail by alkaline lysis method and used for PCR with KOD One (TOYOBO, Osaka, Japan; 98 °C for 10 s, followed by 34 cycles of 98 °C, 64 °C, and 68 °C, respectively, for 10 s, 5 s and 1 s), using primer sets of "F1, F-MUT, R1", "F-target and R-target", "Fot1 and Rot1" and "Fot2 and Rot2" for genotyping, sequencing of the genome editing target region, sequencing of the 2 regions of possible off-target effect (chr5:122,278,836 – 122,278,850 and chr6:31,224,278 – 31,224,292) (Figure S1). PCR products for genotyping (539 bp for *Brca2*^{wt} allele and 419 bp for *Brca2*^{mut} allele) were analyzed by 1% agarose gel electrophoresis. For evaluating the genetic mutations, the 3500xL Genetic Analyzer (Applied Biosystems, Waltham, MA) was used, and potential off-target sequences were identified by CRISPRdirect (https://crispr.dbcls.jp as of June 21st, 2022).

Immunohistochemistry

Immunohistochemical (IHC) staining was carried out on 4-μm-thick formalin-fixed paraffin-embedded (FFPE) specimens using a Leica BOND-MAX (Leica, Bannockburn, IL) with BOND Polymer Detection (ds9800; Leica). Primary antibodies and staining conditions are summarized in Table S2. The images were captured with Cell Sens Dimension software (Olympus) and quantitated using ImageJ Fiji[44].

RNA-sequencing, gene set enrichment analysis and splicing variant analysis

Total RNA was isolated from the testis of 10-week-old *Brca2*$^{wt/wt}$ and *Brca2*$^{wt/mut}$ rats using NucleoSpin RNA Plus kit (#740984, Takara, Japan). RNA library preparation and sequencing were conducted by Rhelixa Co., Ltd (Tokyo, Japan), using NEBNext Poly(A) mRNA Magnetic Isolation Module, NEBNext UltraTMII Directional RNA Library Prep Kit (New England BioLabs, Ipswich, MA), and HiSeq Illumina platform. The quality was assessed with FastQC (Version 0.11.7) and, subsequently, low-quality bases (< 20) and adapter sequences were removed, using Trimmomatic software (Version 0.38). Regarding the analysis of splicing variants, the trimmed reads were analyzed using STAR (Version 2.7.4), QoRTs (Version 1.3.6) and JunctionSeq (Version 3.6.1)[45]. The expression frequency for each exon was normalized by dividing the read count by the length of each exon according to ENSRNOG00000001111. For the pathway analysis, the trimmed reads were analyzed using HISAT2 (Version 2.1.0), Samtools (Version 1.9), featureCounts (Version 1.6.3), DESeq2 (Version 1.24.0) and GSEA (Version 4.3.2)[46,47] with the Rat_Ensembl_Gene_ID_Human_Orthologs_MSigDB.v2023.Hs.chip and gene set databases, including Human Phenotype Ontology and WikiPathways. Visualization was performed using GraphPad Prism (Version 10.0.0; GraphPad Software, Boston, MA) or R Studio[48] with ggplot2 [49]. The original RNA-seq data can be accessed from the DRA (DDBJ Sequence Read Archive) database under the accession code DRA017021, with BioProject Accession: PRJDB16585.

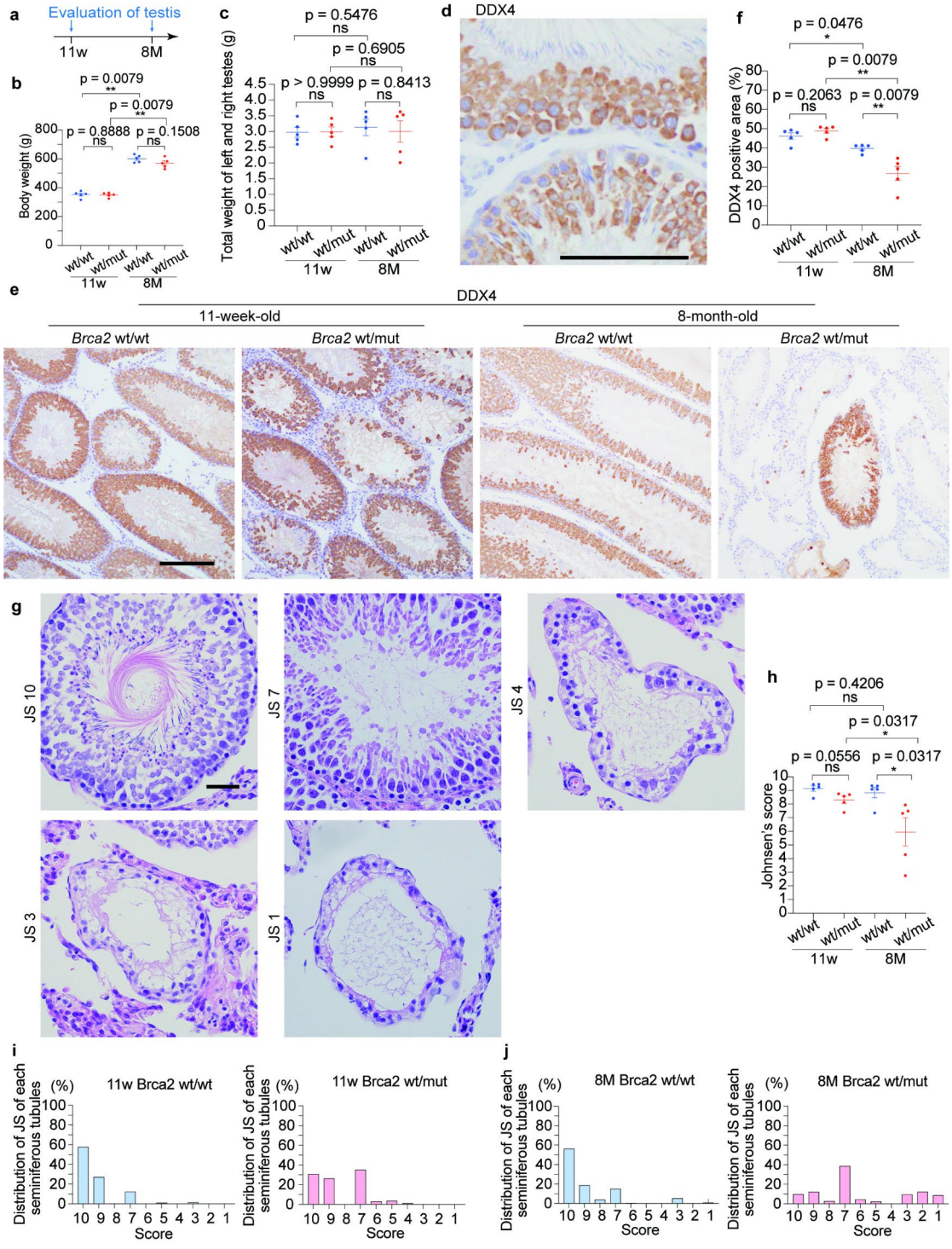

Immunoblot analysis

Testes were lysed in RIPA buffer with cOmplete Mini (Roche, Basel, Switzerland) and PhosSTOP (Roche). The lysates were centrifuged at 18,000 x g for 30 min at 4 °C. The sample proteins were separated by SDS-PAGE using 7.5% polyacrylamide gel and transferred to a PVDF membrane. After blocking with either 5% defatted milk or 3% BSA-TBST, the membranes were incubated with primary antibodies and HRP-conjugated secondary antibodies. The primary antibodies used are summarized in Table S2. Bands were visualized using Chemi-Lumi One Super/Ultra kit (Nakalai Tesque, Kyoto, Japan) and LuminoGraph I (ATTO, Tokyo, Japan). Stripping was performed by agitating the blot in stripping solution (25mM glycine-HCL, 1% SDS, pH 2.0) for 30 min at room temperature, followed by two 5-minute washes with TBST. Reprobing was carried out by blocking, incubation with the primary antibody and secondary antibodies as described above.

◀**Fig. 5**. *Brca2*$^{wt/mut}$male rats reveal accelerated age-dependent decrease in testicular germ cells and Johnsen's score. (**a**) Design of experiments regarding histological assessment of the testis. (**b, c**) Body weight and the weights of testes revealed no significant difference between *Brca2*$^{wt/wt}$ and *Brca2*$^{wt/mut}$ male rats. (**d, e, f**) Representative immunohistochemical images and quantitative analysis of DDX4 in seminiferous tubules ($n=5$; bar = 100 μm). DDX4 is expressed in some population of germ cells, spermatocytes and stage 1–8 spermatids. IHC reveals a significant decrease of DDX4-positive germ cells in *Brca2*$^{wt/mut}$ rats at 8 months. (**g**) Representative histological images for Johnsen's score 10, 7, 4, 3 and 1. Complete spermatogenesis with spermatozoa is classified as score 10, no spermatozoa but many spermatids as score 7, only few spermatocytes with no spermatids as score 4, spermatogonia without the other germ cells as score 3, and no cells in the seminiferous tubule as score 1. (**h**) Comparison of Johnsen's score ($n=5$) revealed that morphologically detectable spermatogenesis disorder is observed in *Brca2*$^{wt/mut}$ testes at 8 months. (**i, j**) Distribution of Johnsen's score in each group. The bars represent the fraction of seminiferous tubules for each Johnsen's score in a total of 500 tubules for each group ($n=5$; 100 tubules per each rat). Seminiferous tubules scored as 7 are abundant in *Brca2*$^{wt/mut}$ at 11 weeks and 8 months. JS, Johnsen's score; ns, not significant.

Johnsen's score

To assess quality of spermatogenesis based on morphology, Johnsen's score was assigned at least to 100 seminiferous tubules in the larger testis of each rat after hematoxylin and eosin staining. The average score for each rat was then calculated (Table S3)[50].

TUNEL assay and quantification of apoptotic cells

Evaluation of apoptotic cells were performed on 4-μm-thick FFPE specimen using MEBSTAIN Apoptosis TUNEL Kit Direct (Medical & Biological Laboratories, Tokyo, Japan) according to the kit manual. Briefly, deparaffinized sections were treated with proteinase K for 30 min at 37 °C, followed by DNA nick end labeling with fluorescein isothiocyanate-dUTP, and counterstaining of nuclei using Hoechst33342 (Thermo Fisher Scientific, MA, USA). Apoptotic cells were observed using SpinSR10 (Olympus Corporation, Tokyo, Japan). Ten images were captured for each sample randomly under 20 times objective lens and the number of germ cells and apoptotic cells were counted.

Sperm parameters

Collection of sperm, evaluation of count, vitality, motility of sperm, and Sperm Chromatin Structure Assay (SCSA) were performed in accordance with WHO recommendation for human sperm[51,52].

Each cauda epididymis was minced by cutting it into ~ 10 fragments with scissors in 1 ml physiological saline, followed by a 30-min incubation at 37 °C. The suspension was gently swirled for 15 s, followed by filtration through a 70-μm strainer. The sperm suspension was maintained 37 °C until motility assessment[51,53].

Vitality was assessed using Eosin-nigrosin staining immediately after the sperm collection. Briefly, 50-μl sperm suspension was mixed with 50-μl eosin-nigrosin solution containing 0.67% eosin Y, 10% nigrosin and 0.9% NaCl. Two min later, 8 μl of the mixture was smeared and air-dried. Counting of alive/dead sperms was performed under microscope immediately after drying, with at least 200 spermatozoa evaluated in each case[51,54].

Sperm motility was recorded using the BZ-X800 (KEYENCE, Osaka, Japan) within 30 min after sperm retrieval. Ten-μl sperm suspension was placed on a slide glass, prewarmed to 37 °C, and observed on a stage of microscope also prewarmed at 37 °C. Five fields were recorded in a 5-sec movie using 20 x objective lens under phase-contrast observation. The sperm were categorized into progressive, non-progressive and immotile. The average of the counts from two slides prepared from the same specimen was considered as the result as described[51,54]. Sperm morphology was classified into the spermatozoa with abnormal head, tailless or abnormal tail[55,56]. At least 100 spermatozoa were evaluated for each rat.

The existence of DNA single and DSBs in sperm nuclei was assessed using acridine orange staining and measured with Sperm Chromatin Structure Assay (SCSA) within 6 h after sperm collection[51,57]. Briefly, 5 μl of sperm suspension was transferred into 200-μl TNE buffer (0.876% NaCl, 0.01 M Tris-HCl, 1mM EDTA, pH 7.4, DW), followed by an addition of 400-μl acid detergent solution (0.08 N HCl, 0.15 M NaCl, 0.1% Triton X-100, pH 1.20) and vortexed. After 30 s, 1,200-μl Acridine Orange (AO) staining solution (0.0006% AO, 0.1 M citric acid buffer, 0.2 M Na_2HPO_4, DW) was added and mixed. After 3-min incubation, the fluorescence was evaluated with BZ-X800 or DxFLEX flow cytometer (Beckman Coulter, Inc.; Brea, CA).

Statistical analysis

Statistical analysis of trends in litter size was conducted using a paired *t*-test. The other analyses involving IHC and sperm parameters were performed using the *Mann-Whitney U*-test, due to the small sample size and difficulty in ensuring normal distribution. The analyses were carried out using GraphPad Prism10.0.0 with two-tailed testing. Error bars are shown as means ± SEM.

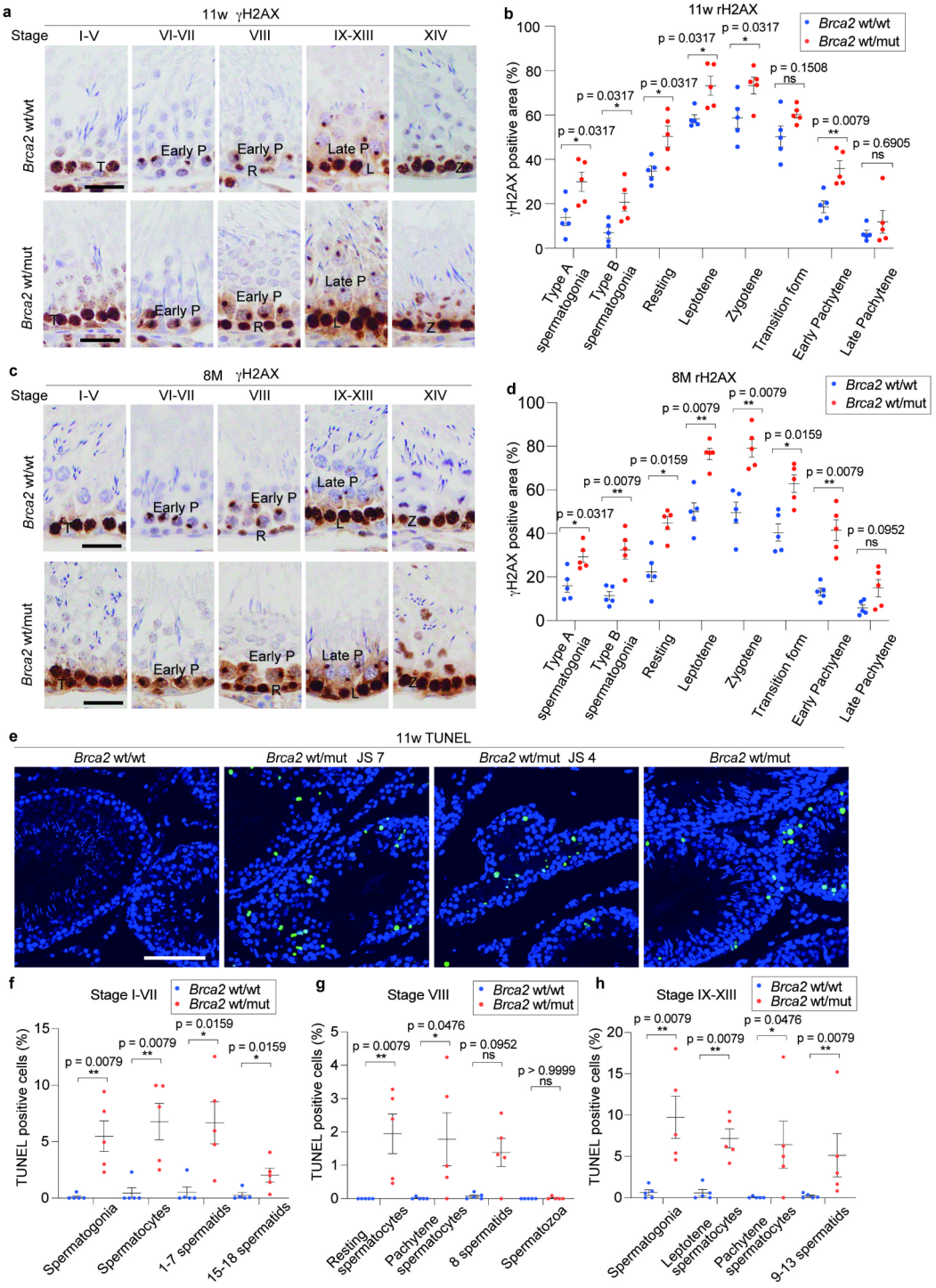
a
11w γH2AX
Stage
I-V
VI-VII
VIII
IX-XIII
XIV
Brca2 wt/wt
Brca2 wt/mut
Early P
Late P
b
11w rH2AX
Brca2 wt/wt
Brca2 wt/mut
γH2AX positive area (%)
p = 0.0317
p = 0.1508
ns
p = 0.0079
p = 0.6905
Type A spermatogonia
Type B spermatogonia
Resting
Leptotene
Zygotene
Transition form
Early Pachytene
Late Pachytene
c
8M γH2AX
d
8M rH2AX
p = 0.0159
p = 0.0952
e
11w TUNEL
Brca2 wt/wt
Brca2 wt/mut JS 7
Brca2 wt/mut JS 4
Brca2 wt/mut
f
Stage I-VII
TUNEL positive cells (%)
Spermatogonia
Spermatocytes
1-7 spermatids
15-18 spermatids
g
Stage VIII
p = 0.0476
p > 0.9999
Resting spermatocytes
Pachytene spermatocytes
8 spermatids
Spermatozoa
h
Stage IX-XIII
Spermatogonia
Leptotene spermatocytes
Pachytene spermatocytes
9-13 spermatids

◀**Fig. 6**. *Brca2*$^{wt/mut}$ testicular germ cells exhibit accumulation of DNA double-strand break and increased apoptosis. (**a, b, c, d**) Representative immunohistochemical images and quantitative analysis of γH2AX in spermatogonia and spermatocytes classified in type A spermatogonia (stage IX-XIV), type B spermatogonia (stage IV-VI), resting form (stage VIII), leptotene (stage IX-XIII), zygotene (stage XIV), transition form (stage I-V), early pachytene (stage VI-VIII) and late pachytene (stage IX-XIII) ($n = 5$, with at least 10 fields taken randomly with x20 magnification were analyzed per individual, bar = 30 μm,). In spermatogonia and spermatocyte of *Brca2*$^{wt/mut}$ rats at 11 weeks and 8 months, accumulation of DNA double strand breaks is observed throughout the differentiation stages. R, resting spermatocytes; L, leptotene; T, transition form; P, pachytene; DI, diplotene and diakinesis; M, metaphase. (**e**) Representative images of TUNEL-staining in seminiferous tubules. *Brca2*$^{wt/wt}$ seminiferous tubules contained scarce TUNEL-positive cells (bar = 100 μm). On the other hand, *Brca2*$^{wt/mut}$ seminiferous tubules contained higher population of TUNEL-positive cells, especially in seminiferous tubules classified as JS-7 or lower. (**f, g, h**) Analysis of TUNEL-positive rate of germ cells within seminiferous tubules at each stage, excluding seminiferous tubules classified as JS-7 or lower. This analysis revealed that, compared to *Brca2*$^{wt/wt}$, *Brca2*$^{wt/mut}$ exhibited increased apoptosis in spermatogonia, spermatocytes, and spermatids at all stages of seminiferous tubules.

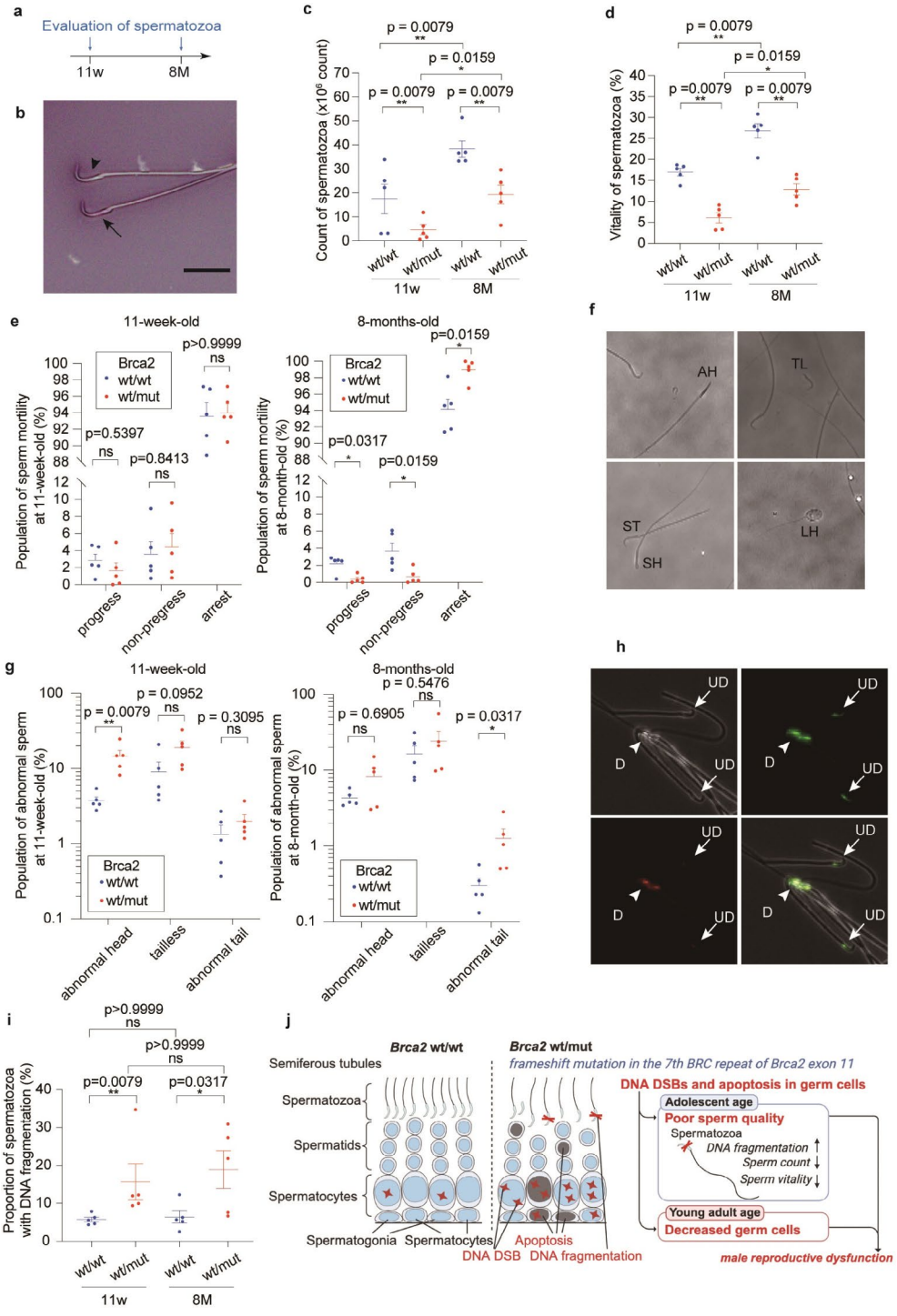

Fig. 7. *Brca2*$^{wt/mut}$ male rats reveal deteriorated sperm quality. (**a**) Design of experiments regarding the characterization of spermatozoa. (**b**) Representative images of Eosin Y-Nigrosin staining (bar = 20 μm; arrowhead, viable spermatozoa; arrow, dead spermatozoa). (**c**) Number of spermatozoa and (**d**) vitality of spermatozoa are decreased in *Brca2*$^{wt/mut}$ group both at 11 weeks and 8 months ($n = 5$). (**e**) Motility of sperms from *Brca2*$^{wt/mut}$ rats is not deteriorated at 11 weeks but decreased at 8 months ($n = 5$). (**f**) Representative morphology of abnormal sperms. AH, abnormal head sperm; TL, tailless sperm; ST, short tail sperm; SH, small head sperm; LH, large head sperm. (**g**) Abnormal sperm was more abundant in *Brca2*$^{wt/mut}$ than *Brca2*$^{wt/wt}$ both at 11 weeks and 8 months. (**h**) Representative images of the sperms stained with acridine orange (arrowhead, damaged sperm DNA as D; arrow, undamaged sperm DNA as UD). (**i**) Comparison of the proportion of spermatozoa with DNA fragmentation within a sperm sample detected from SCSA ($n = 5$). This proportion of spermatozoa with DNA fragmentation is commonly referred to as DNA fragmentation index, DFI. Both at 11 weeks and 8 months, the spermatozoa of the *Brca2*$^{wt/mut}$ rats show more DNA fragmentation than those of *Brca2*$^{wt/wt}$. SCSA, sperm chromatin structure assay. (**j**) Summary of the findings.

Gender	Name	Mutational pattern	Number of births at first childbirth (inheritance rates of mutant Brca2 alleles (%))
Male	#3	g.16,596_16,603del, c.5,821_5,828del p.R1,941Wfs*3	No pups
Male	#18	g.16,600_16,622del, c.5,825_5,847del, p.T1,942Kfs*8	6 males and 7 females (p.T1,942Kfs*8: 53.8%)
Male	#19	g.16,572_16,621del, c.5,817_5,846del, p.K1,928Nfs*2 g.16,600_16,617del, c.5,825_5,842del, p.T1,942_S1,947del	6 males and 6 females (p.K1,928Nfs*2: 41.7%) (p.T1,942_S1,947del: 58.3%)
Male	#27	g.16,600_16,622del, c.5,825_5,847del, p.T1,942Kfs*8	7 males and 12 females (p.T1,942Kfs*8: 52.9%)
Female	#6	g.16,594_16,610del, c.5,819_5,835del, p.S1,940Ffs*1 g.16,601_16,618del, c.5,826_5,843del, p.Y1,943_T1,948del	7 males and 8 females (p.S1,940Ffs*1: 40.0%) (p.Y1,943_T1,948del: 60.0%)
Female	#7	g.16,611_16,630delinsA, c.5,836_5,855delinsA, p.Y1,943Qfs*22 g.16,601_16,618del, c.5,826_5,843del, p.Y1,943_T1,948del	No pups
Female	#9	g.16,556_16,605del, c.5,781_5,830del, p.C1,927Wfs*3 g.16,601_16,618del, c.5,826_5,843del, p.Y1,943_T1,948del	8 males and 5 females (p.C1,927Wfs*3: 7.7%) (p.Y1,943_T1,948del : 53.8%)
Female	#16	g.16,611_16,909del, c.5,836_6,134del, p.G1,944Ifs*6	4 males and 3 females (p.G1,944Ifs*6: 0%)
Female	#24	g.16,601_16,609delinsA, c.5,826_5,834del, p.Y1,943Ffs*1 g.16,589_16,605del, c.5,814_5,830del, p.H1,938Qfs*3	5 males and 3 females (p.Y1,943Ffs*1: 25.0%) (p.H1,938Qfs*3: 25.0%)
Female	#26	g.16,596_16,608del, c.5,821_5,833del, p.R1,941Ffs*26 g.16,598_16,603del, c.5,823_16,605del, p.T1,942_Y1,943del	2 males and 2 females (p.R1,941Ffs*26: 25.0%) (p.T1,942_Y1,943del: 0%)

Table 1. Summary of mutant alleles in founder rats and the prevalence rate to F1 generation.

Data availability

All original RNA-seq data generated in this study have been deposited in DRA (DDBJ Sequence Read Archive) database under the accession code DRA017021, with BioProject Accession: PRJDB16585. All other data supporting the finding of this study are available in the article or its supramental files. Any additional requests for information will be fulfilled by corresponding author.

Received: 18 September 2024; Accepted: 20 December 2024
Published online: 02 January 2025

References

1. McAllister, K. A. et al. Characterization of the rat and mouse homologues of the BRCA2 breast cancer susceptibility gene. *Cancer Res.* **57**, 3121–3125 (1997).
2. Roy, R., Chun, J. & Powell, S. N. BRCA1 and BRCA2: different roles in a common pathway of genome protection. *Nat. Rev. Cancer.* **12**, 68–78. https://doi.org/10.1038/nrc3181 (2011).
3. Kwon, Y. et al. DNA binding and RAD51 engagement by the BRCA2 C-terminus orchestrate DNA repair and replication fork preservation. *Nat. Commun.* **14**, 432. https://doi.org/10.1038/s41467-023-36211-x (2023).
4. Davies, O. R. & Pellegrini, L. Interaction with the BRCA2 C terminus protects RAD51-DNA filaments from disassembly by BRC repeats. *Nat. Struct. Mol. Biol.* **14**, 475–483. https://doi.org/10.1038/nsmb1251 (2007).
5. Momozawa, Y. et al. Germline pathogenic variants of 11 breast cancer genes in 7,051 Japanese patients and 11,241 controls. *Nat. Commun.* **9**, 4083. https://doi.org/10.1038/s41467-018-06581-8 (2018).
6. Maxwell, K. N., Domchek, S. M., Nathanson, K. L. & Robson, M. E. Population frequency of germline BRCA1/2 mutations. *J. Clin. Oncol.* **34**, 4183–4185. https://doi.org/10.1200/JCO.2016.67.0554 (2016).
7. Magraner-Pardo, L., Laskowski, R. A., Pons, T. & Thornton, J. M. A computational and structural analysis of germline and somatic variants affecting the DDR mechanism, and their impact on human diseases. *Sci. Rep.* **11**, 14268. https://doi.org/10.1038/s41598-021-93715-6 (2021).
8. Labidi-Galy, S. I. et al. Location of mutation in BRCA2 gene and survival in patients with ovarian Cancer. *Clin. Cancer Res.* **24**, 326–333. https://doi.org/10.1158/1078-0432.CCR-17-2136 (2018).
9. Fiesco-Roa, M. O., Giri, N., McReynolds, L. J., Best, A. F. & Alter, B. P. Genotype-phenotype associations in fanconi anemia: a literature review. *Blood Rev.* **37**, 100589. https://doi.org/10.1016/j.blre.2019.100589 (2019).
10. Alter, B. P., Rosenberg, P. S. & Brody, L. C. Clinical and molecular features associated with biallelic mutations in FANCD1/BRCA2. *J. Med. Genet.* **44**, 1–9. https://doi.org/10.1136/jmg.2006.043257 (2007).
11. Momozawa, Y. et al. Expansion of Cancer Risk Profile for BRCA1 and BRCA2 pathogenic variants. *JAMA Oncol.* **8**, 871–878. https://doi.org/10.1001/jamaoncol.2022.0476 (2022).
12. Vander Borght, M. & Wyns, C. Fertility and infertility: definition and epidemiology. *Clin. Biochem.* **62**, 2–10. https://doi.org/10.1016/j.clinbiochem.2018.03.012 (2018).
13. Horton, R., Pharoah, P., Hayward, J. & Lucassen, A. Care of men with cancer-predisposing BRCA variants. *BMJ* **375**, n2376. https://doi.org/10.1136/bmj.n2376 (2021).
14. Cotroneo, M. S. et al. Characterizing a rat Brca2 knockout model. *Oncogene* **26**, 1626–1635. https://doi.org/10.1038/sj.onc.1209960 (2007).
15. Sharan, S. K. et al. Embryonic lethality and radiation hypersensitivity mediated by Rad51 in mice lacking Brca2. *Nature* **386**, 804–810. https://doi.org/10.1038/386804a0 (1997).
16. Sharan, S. K. et al. BRCA2 deficiency in mice leads to meiotic impairment and infertility. *Development* **131**, 131–142. https://doi.org/10.1242/dev.00888 (2004).
17. Zhang, J. et al. The BRCA2-MEILB2-BRME1 complex governs meiotic recombination and impairs the mitotic BRCA2-RAD51 function in cancer cells. *Nat. Commun.* **11**, 2055. https://doi.org/10.1038/s41467-020-15954-x (2020).

18. Brandsma, I. et al. HSF2BP Interacts with a Conserved Domain of BRCA2 and Is Required for Mouse Spermatogenesis. *Cell Rep* **27**, 3790–3798 e3797. https://doi.org/10.1016/j.celrep.2019.05.096 (2019).
19. Takemoto, K. et al. Meiosis-specific C19orf57/4930432K21Rik/BRME1 modulates localization of RAD51 and DMC1 to DSBs in mouse meiotic recombination. *Cell. Rep.* **31**, 107686. https://doi.org/10.1016/j.celrep.2020.107686 (2020).
20. Ghouil, R. et al. BRCA2 binding through a cryptic repeated motif to HSF2BP oligomers does not impact meiotic recombination. *Nat. Commun.* **12**, 4605. https://doi.org/10.1038/s41467-021-24871-6 (2021).
21. Schneider, B. F. & Norton, S. Equivalent ages in rat, mouse and chick embryos. *Teratology* **19**, 273–278. https://doi.org/10.1002/tera.1420190302 (1979).
22. Furukawa, S., Tsuji, N. & Sugiyama, A. Morphology and physiology of rat placenta for toxicological evaluation. *J. Toxicol. Pathol.* **32**, 1–17. https://doi.org/10.1293/tox.2018-0042 (2019).
23. Leblond, C. P. & Clermont, Y. Definition of the stages of the cycle of the seminiferous epithelium in the rat. *Ann. N Y Acad. Sci.* **55**, 548–573. https://doi.org/10.1111/j.1749-6632.1952.tb26576.x (1952).
24. Sengupta, P. The Laboratory Rat: relating its Age with Human's. *Int. J. Prev. Med.* **4**, 624–630 (2013).
25. Lewis, E. M., Barnett, J. F., Freshwater, L., Hoberman, A. M. & Christian, M. S. Sexual Maturation Data for Crl Sprague-Dawley rats: Criteria and confounding factors. *Drug Chem. Toxicol.* **25**, 437–458. https://doi.org/10.1081/dct-120014794 (2002).
26. Toyokuni, S. et al. Quantitative immunohistochemical determination of 8-hydroxy-2'-deoxyguanosine by a monoclonal antibody N45.1: its application to ferric nitrilotriacetate-induced renal carcinogenesis model. *Lab. Invest.* **76**, 365–374 (1997).
27. Toyokuni, S. et al. The monoclonal antibody specific for the 4-hydroxy-2-nonenal histidine adduct. *FEBS Lett.* **359**, 189–191. https://doi.org/10.1016/0014-5793(95)00033-6 (1995).
28. Vilenchik, M. M., Knudson, A. G. & Endogenous DNA double-strand breaks: production, fidelity of repair, and induction of cancer. *Proc. Natl. Acad. Sci. U S A.* **100**, 12871–12876. https://doi.org/10.1073/pnas.2135498100 (2003).
29. Esteves, S. C. et al. Sperm DNA fragmentation testing: Summary evidence and clinical practice recommendations. *Andrologia* **53**, e13874. https://doi.org/10.1111/and.13874 (2021).
30. Blake, J. A., Kadin, B. R., Richardson, J. A., Smith, J. E. & Bult, C. L. CJ; Mouse Genome Database Group. Mouse Genome Database (MGD): Knowledgebase for mouse-human comparative biology (2021).
31. OECD. Test No. 451: Carcinogenicity Studies (2018).
32. Zan, Y. et al. Production of knockout rats using ENU mutagenesis and a yeast-based screening assay. *Nat. Biotechnol.* **21**, 645–651. https://doi.org/10.1038/nbt830 (2003).
33. Mesman, R. L. S. et al. Alternative mRNA splicing can attenuate the pathogenicity of presumed loss-of-function variants in BRCA2. *Genet. Med.* **22**, 1355–1365. https://doi.org/10.1038/s41436-020-0814-5 (2020).
34. Thompson, D. & Easton, D. Breast Cancer linkage, C. Variation in cancer risks, by mutation position, in BRCA2 mutation carriers. *Am. J. Hum. Genet.* **68**, 410–419. https://doi.org/10.1086/318181 (2001).
35. Xia, F. et al. Deficiency of human BRCA2 leads to impaired homologous recombination but maintains normal nonhomologous end joining. *Proc. Natl. Acad. Sci. U S A.* **98**, 8644–8649. https://doi.org/10.1073/pnas.151253498 (2001).
36. Chen, C. F., Chen, P. L., Zhong, Q., Sharp, Z. D. & Lee, W. H. Expression of BRC repeats in breast cancer cells disrupts the BRCA2-Rad51 complex and leads to radiation hypersensitivity and loss of G(2)/M checkpoint control. *J. Biol. Chem.* **274**, 32931–32935. https://doi.org/10.1074/jbc.274.46.32931 (1999).
37. Evers, B. & Jonkers, J. Mouse models of BRCA1 and BRCA2 deficiency: past lessons, current understanding and future prospects. *Oncogene* **25**, 5885–5897. https://doi.org/10.1038/sj.onc.1209871 (2006).
38. Utsuno, H., Oka, K., Yamamoto, A. & Shiozawa, T. Evaluation of sperm head shape at high magnification revealed correlation of sperm DNA fragmentation with aberrant head ellipticity and angularity. *Fertil. Steril.* **99**, 1573–1580. https://doi.org/10.1016/j.fertnstert.2013.01.100 (2013).
39. Cohen-Bacrie, P. et al. Correlation between DNA damage and sperm parameters: a prospective study of 1,633 patients. *Fertil. Steril.* **91**, 1801–1805. https://doi.org/10.1016/j.fertnstert.2008.01.086 (2009).
40. Yang, H., Li, G., Jin, H., Guo, Y. & Sun, Y. The effect of sperm DNA fragmentation index on assisted reproductive technology outcomes and its relationship with semen parameters and lifestyle. *Transl Androl. Urol.* **8**, 356–365. https://doi.org/10.21037/tau.2019.06.22 (2019).
41. Liu, K., Mao, X., Pan, F., Chen, Y. & An, R. Correlation analysis of sperm DNA fragmentation index with semen parameters and the effect of sperm DFI on outcomes of ART. *Sci. Rep.* **13**, 2717. https://doi.org/10.1038/s41598-023-28765-z (2023).
42. Belloc, S. et al. Sperm deoxyribonucleic acid damage in normozoospermic men is related to age and sperm progressive motility. *Fertil. Steril.* **101**, 1588–1593. https://doi.org/10.1016/j.fertnstert.2014.02.006 (2014).
43. Braga, D. et al. The effect of sperm DNA fragmentation on ICSI outcomes depending on oocyte quality. *Andrology* **11**, 1682–1693. https://doi.org/10.1111/andr.13435 (2023).
44. Schindelin, J. et al. Fiji: an open-source platform for biological-image analysis. *Nat. Methods.* **9**, 676–682. https://doi.org/10.1038/nmeth.2019 (2012).
45. Hartley, S. W. & Mullikin, J. C. Detection and visualization of differential splicing in RNA-Seq data with JunctionSeq. *Nucleic Acids Res.* **44**, e127. https://doi.org/10.1093/nar/gkw501 (2016).
46. Subramanian, A. et al. Gene set enrichment analysis: a knowledge-based approach for interpreting genome-wide expression profiles. *Proc. Natl. Acad. Sci. U S A.* **102**, 15545–15550. https://doi.org/10.1073/pnas.0506580102 (2005).
47. Mootha, V. K. et al. PGC-1alpha-responsive genes involved in oxidative phosphorylation are coordinately downregulated in human diabetes. *Nat. Genet.* **34**, 267–273. https://doi.org/10.1038/ng1180 (2003).
48. Team, R. *RStudio Integrated Development for R. RStudio* (PBC, Boston, 2020).
49. H, W. *ggplot2: Elegant Graphics for Data Analysis* (Springer-Verlag New York, 2016). ISBN 978-3-319-24277-4.
50. Johnsen, S. G. Testicular biopsy score count–a method for registration of spermatogenesis in human testes: normal values and results in 335 hypogonadal males. *Hormones* **1**, 2–25. https://doi.org/10.1159/000178170 (1970).
51. Organization, W. H. *WHO laboratory manual for the examination and processing of human semen* 6th edn (Geneva, 2021) Report No. 978-92-4-003078-7.
52. Baldi, E. et al. Extended semen examinations in the sixth edition of the WHO Laboratory Manual for the examination and Processing of Human Semen: contributing to the understanding of the function of the male reproductive system. *Fertil. Steril.* **117**, 252–257. https://doi.org/10.1016/j.fertnstert.2021.11.034 (2022).
53. Oyovwi, M. O., Oghenetega, O. B., Victor, E., Faith, F. Y. & Uchechukwu, J. G. Quercetin protects against levetiracetam induced gonadotoxicity in rats. *Toxicology* **491**, 153518. https://doi.org/10.1016/j.tox.2023.153518 (2023).
54. Turk, G., Atessahin, A., Sonmez, M., Ceribasi, A. O. & Yuce, A. Improvement of cisplatin-induced injuries to sperm quality, the oxidant-antioxidant system, and the histologic structure of the rat testis by ellagic acid. *Fertil. Steril.* **89**, 1474–1481. https://doi.org/10.1016/j.fertnstert.2007.04.059 (2008).
55. Sharma, P. & Singh, R. Protective role of curcumin on lindane induced reproductive toxicity in male Wistar rats. *Bull. Environ. Contam. Toxicol.* **84**, 378–384. https://doi.org/10.1007/s00128-010-9942-y (2010).
56. Narayana, K., D'Souza, U. J. & Seetharama Rao, K. P. Ribavirin-induced sperm shape abnormalities in Wistar rat. *Mutat. Res.* **513**, 193–196. https://doi.org/10.1016/s1383-5718(01)00308-4 (2002).
57. Evenson, D. P. Sperm chromatin structure assay (SCSA(R)) for Fertility Assessment. *Curr. Protoc.* **2**, e508. https://doi.org/10.1002/cpz1.508 (2022).

Acknowledgements
We thank the Division for Medical Research Engineering in Nagoya University Graduate School of Medicine for DxFLEX usage, Nobuaki Misawa and Megumi Akiyama from Nagoya University, Japan, for their assistance with animal experiments and tissue work, and Ryo Nakaki and M. Kawamura from Rhelixa, Inc., Japan, for RNA-seq data analysis. We created illustrations in Figs. 1a and 3c L with BioRender.com.

Author contributions
Y. Mo. and S.T. conceived and, along with T.M., designed the animal model. T.M. engineered the founder rats, whereas Y. Mo., H.T. and Y. Ma. established the rat strain. Y. Mo. collected reproductive data, conducted formal analyses, including RNA-seq, and managed the project. Y. Mo. drafted the manuscript, which S.T. reviewed and edited, followed by critical review from all the other authors.

Funding
Supported in part by JSPS Kakenhi JP23K08883 to Y. Motooka, and JST CREST (JPMJCR19H4) and JSPS Kakenhi (JP19H05462 and JP16H06276 [AdAMS (Aa210038)]) to ST.

Declarations

Competing interests
The authors declare no competing interests.

Additional information
Supplementary Information The online version contains supplementary material available at https://doi.org/10.1038/s41598-024-84184-8.

Correspondence and requests for materials should be addressed to Y.M. or S.T.